Asian Journal of Applied Chemistry Research

Volume 15, Issue 4, Page 172-193, 2024; Article no.AJACR.123758
ISSN: 2582-0273

Optimization of Tantalite Ore Dissolution Using Hydrofluoric-sulphuric Acid and Shrinking Core Model

Agho, Timothy Imuetinyan [a*], Okuo, James Majebi [b] and Emeribe, Favour Oluchi [b]

[a] Department of Science Laboratory Technology, Faculty of Life Sciences, University of Benin, Benin City, Nigeria.
[b] Analytical and Environmental Research Laboratory, Department of Chemistry, Faculty of Physical Sciences, University of Benin, Benin City, Nigeria.

Authors' contributions

This work was carried out in collaboration among all authors. All authors read and approved the final manuscript.

Article Information

DOI: https://doi.org/10.9734/ajacr/2024/v15i4305

Open Peer Review History:
This journal follows the Advanced Open Peer Review policy. Identity of the Reviewers, Editor(s) and additional Reviewers, peer review comments, different versions of the manuscript, comments of the editors, etc are available here: https://www.sdiarticle5.com/review-history/123758

Original Research Article

Received: 21/07/2024
Accepted: 23/09/2024
Published: 01/10/2024

ABSTRACT

Aim: This study investigates the dissolution of tantalite mineral from granitic pegmatite in Okpella, Northern Edo State, Nigeria.
Study Design: Elemental and mineral composition analysis of tantalite ore sample from Okpella was carried out using X-ray fluorescence and X-ray diffraction. Response Surface Methodology

**Corresponding author: Email: timothy.agho@uniben.edu;*

Cite as: *Agho, Timothy Imuetinyan, Okuo, James Majebi, and Emeribe, Favour Oluchi. 2024. "Optimization of Tantalite Ore Dissolution Using Hydrofluoric-Sulphuric Acid and Shrinking Core Model". Asian Journal of Applied Chemistry Research 15 (4):172-93. https://doi.org/10.9734/ajacr/2024/v15i4305.*

(RSM) and the shrinking core model were used in designing the study while the effects of temperature, stirring speed, particle diameter, and mixed acids concentrations were investigated in the dissolution rates of the mineral.
Duration of Study: 50 experimental runs were designed using RSM Central Composite Design (CCD) to optimize variables including HF concentration (1-8 M), H2SO4 concentration (0.5-3 M), temperature (32-82°C), stirring speed (0-500 rpm), and particle size (0.1-0.3 mm), with a constant contact time of 240 minutes.
Methodology: Pulverized tantalite samples (0.1-0.3 mm) were reacted with varying concentrations of hydrofluoric and sulphuric acids (1-8 M and 0.5-3.0 M, respectively) for 240 minutes, with stirring speeds between 0-500 rpm and temperatures from 32 to 82°C. The mixture was stirred in a water bath with 50 ml of mixed acids solution and 2 g of ore. After the reaction, the solution was decanted, and the residual ore was washed, dried at 60 °C, and weighed. The difference between the initial and final weights indicated the amount of undissolved tantalite ore.
Results: Ore characterization results revealed high concentration of tantalum (34.17%), iron (12.55%), niobium (8.38%), and titanium (6.01%), with other elements present in smaller amounts. Optimal conditions were found to be 8 M HF, 0.5 M H2SO4, 82°C, 500 rpm stirring speed, and 0.1 mm particle size, resulting in 97.28% dissolution of tantalite ore. Regression analysis demonstrated model robustness with an F-value of 16.70 and a P-value of 0.0001, indicating HF concentration and stirring speed as the most impactful factors. The model's R^2 value of 0.9201 and adjusted R^2 of 0.8650 confirm its predictive accuracy. Analysis using the shrinking sphere model showed that film diffusion control is the primary limiting step with $t/\tau=0.999$, while reaction control resulted in slightly lower conversion with $t/\tau=0.973$, highlighting film diffusion as the main constraint but with high conversion efficiency.
Conclusion: The findings from this investigation not only reveal the dissolution of tantalite ore through a detailed experimental approach, identifying optimal conditions -8 M HF, 0.5 M H2SO4, 82 oC, 500 rpm stirring speed and 0.1 mm particle size- that achieve a 97.28% dissolution, but they also enhance our understanding of mineral processing. These understanding are crucial for mineral dissolution up scaling technologies in industrial applications, which will potentially leads to a more efficient extraction method that could significantly reduce costs and environmental impacts in the mining sector. This research could drive advancements in sustainable resource recovery and contribute to sourcing of critical minerals.

Keywords: Dissolution; tantalite ore; response surface methodology; shrinking core model.

1. INTRODUCTION

The economic value of tantalite ore stems from its role as the primary source of the metals niobium and tantalum. It is a group of minerals with the general formula (Fe, Mn) $(Ta, Nb)_2O_6$. Tantalite is chemically similar to columbite, and the two are often grouped together as a semi-singular mineral called coltan or "columbite-tantalite" in many mineral guides [1,2]. However, tantalite has a much greater specific gravity than columbite [3-5]. Other elements found associated with the ore include tin, manganese, iron, germanium and tungsten [6]. Tantalite itself isn't found in nature as a pure mineral; they are found in granite pegmatites that are rich in rare-earth elements and are also present in placer deposits derived from such rocks [7]. According to Sons of Gwalia fourth quarter report 2004, Western Australia contributed significantly to the global supply of tantalum, with Sons of Gwalia Limited's Greenbushes' and Woodgina mines being the world's single largest producer of tantalum mineral concentrate.

Generally, tantalum recycling primarily targets tantalum-containing components from electronic devices, alongside new and used scrap generated during the production of tantalum-based cemented carbides and superalloys. The efficiency of tantalum recycling varies considerably across different applications and with the specific recycling technology employed. Over the years researchers have demonstrated the potential for significant improvement, with certain methods achieving tantalum recovery rates exceeding 50% from specific waste streams. Challenges hindering wider adoption of tantalum recycling include the complexity of separating tantalum from mixed electronic waste streams, the presence of contaminants, and economic considerations [8]. Apparently, there is little or no report on optimization of tantalite ore dissolution in hydrofluoric-sulphuric acid using

response surface methodology and the shrinking core model. However, Baba et al. (2015) reported on the kinetics of the dissolution of a Nigerian tantalite ore in hydrochloric acid [9].

Investigation of dissolution kinetics of a Nigerian columbite in hydrofluoric acid using the shrinking core model were reported by Olusola and Folarin [10] and Sanda and Taiwo [11]. The extraction of tantalum is more selective for hydrofluoric-sulphuric acid solution preventing co-extraction of other metals having chloro-complexs. The complexation of fluoride ions (F^-) which readily complex with tantalum ($Ta^{\delta+}$) to form soluble fluoro-tantalate complexes (TaF^{6-}) remain dissolved in the leachate solution, The chloride complexes of other metals form a weak or insoluble complexes with chlorides ions (Cl^-) present in hydrochloric acid (HCl) [12]. The sulphuric acid (H_2SO_4) plays a supporting role in this process. It helps dissolve the gangue minerals (impure rock surrounding the tantalite) and maintains the acidity of the solution, favouring the formation of fluorotantalate complexes [13]. The high acidity suppresses the hydrolysis of metal cations like Fe^{2+} and Mo^{6+}; further reducing their tendency to form precipitates.

According Nishumura, et al. [14], 96% of tantalum was extracted into MIBK and niobium was only 2% using 1 M hydrofluoric acid and 0.5 M sulphuric acid indicating the efficiency of hydrofluoric-sulphuric acid in tantalum extraction from leached tantalite. Okuo and Agho [15] reported a preliminary survey of the lithochemistry of tantalite mineral from granitic pegmatite deposits in the Okpella area, Northern Edo State, Nigeria. The analysis revealed a significant presence of tantalum oxide, Ta_2O_5 (41.72%) and other useful oxides of niobium, Nb_2O_5 (11.98%), titanium, TiO_2 (10.02%), iron, Fe_2O_3 (17.94%), magnesium, MgO (6.00%), silicon, (4.35%), manganese, MnO_2 (2.75%), and aluminium, Al_2O_3, (1.52%) with impurity elements such as calcium, potassium, chromium, sodium, phosphorus, tin, tungsten and thorium. Stanislanus et al. [16] reported the pyrometallurgical approach in the recovery of niobium and tantalum. The study shows the conventional reduction of Nb and Ta mineral or Nb_2O_5 and Ta_2O_5 to Nb and Ta metal and with low success in the process and factors responsible for these challenges. Neta et al. [17] reported the characterization and alternative dissolution of tantalite mineral samples from Mozambique and the results shows complete dissolution using $Li_2B_4O_7$. Results from the investigation shows the recovery of 98.52% Nb_2O_5 and 100.43% Ta_2O_5. According to Berhe et al. [18], after investigating the decomposition of the Kenticha mangano-tantalite ore by HF/H_2SO_4 and KOH fusion. Found out that there was no significant change in the leaching rate of Tantalum and Niobium beyond 50^{o}C for the HF/H_2SO_4 system and above 400^{o}C when using the KOH fusion process. Berhe and Cheru [19] further investigated the hydrometallurgical assessment of oxides of Nb, Ta, Th and U from Ethiopian tantalite ore. Data from the study reveal a successive beneficiation of the pigmatites ore with higher dissolution of 60.83 wt% of Ta2O5 with 4.58 wt% of Nb_2O_5 including the removal of U, Th, Ti, Fe and Si with the % lower weight. The concentrated ore was leached with a mixture of binary acids HF and H_2SO_4 with 6:1 ratio at temperatures from 100 to 400 ^{o}C. Also, Guo et al. [20] studied the surface structure change of columbite-(Fe) dissolution in H_2SO_4. The results revealed that Nb dissolution from Columbite-(Fe) occurred more easily compared to Fe. Nb dissolution from the mineral was owed to the content of H+ in solution, and increasing the H+ concentration could promote the dissolution.

Researchers over the years have developed several methods of obtaining or extracting tantalum in various materials [21]. Their objectives likely encompass the identification of key physicochemical parameters governing efficient tantalum leaching and the development of methodologies for selective separation of tantalum from co-extracted impurities, particularly niobium and tungsten. This research work present a detailed study on the application of the hydrofluoric-sulphuric acid for the dissolution of tantalite ore using response surface method and the shrinking core model in optimizing the process of leaching and reaction rate. To the best of our knowledge, no detailed work on the dissolution of tantalite ore from Okpella, Edo State Nigerian has been reported.

2. MATERIALS AND METHODS

2.1 Materials and Reagents

Tantalite ore obtained from Okpella in Etsako East Local Government Area of Edo State Nigeria was used for this study. The reagents used for this research work are mainly of analytical grade from Avantor Sciences. Distilled-

deionized water was used for the preparation of all hydrofluoric-sulphuric acid solutions.

2.1.1 Instrumentations

The elemental and compound analysis of tantalite ore was carried out using 702HS Shimadzu (EDXRF) x-ray fluorescence and a 240OH Shimadzu x-ray diffraction spectrometry [22]. The Joan laboratory thermostatic water bath with magnetic stirrer model WB-6S/WBS-6pro was used for stirring solution. A 500 ml iplusmile plastic Erlenmeyer conical flask and sieve of various sizes ranges from 0.063-4.0 mm were used for the solution preparation for the experiments.

2.1.2 Response Surface Methodology (RSM)

RSM is a multivariant statistical and mathematical procedure that can be applied to the model to understand and give an experimental insight when a response of significance is determined by multiple variables. The design-Expert software (version 13) from Stat-Ease, Inc. was used for the experimental design. The process parameters were modeled using response surface methodology (RSM) with a central composite design (CCD). Five independent variables of acids concentrations, temperature, stirring speed and particle diameters, leading to 50 dissolution runs, were generated (Table 4). The dissolution temperature, HF and H_2SO_4 concentrations, stirring speed, and particle diameters were varied, coupled with a constant dissolution time of 240 minutes. After the 50 experimental CCD tests, the experimental percentage of dissolved tantalite ore was displayed via the RSM. Using analysis of variance (ANOVA), the significance and suitability of the variables can be verified [23,24]. With the linear model developed from the Design of Experiment, the effect of the relationships between the five factors and their direct effect on the percentage dissolution of tantalite ore were determined. Then, the desirability function was used to derive optimal dissolution parameters to increase the leaching of the ore.

2.1.3 Shrinking Core Model (SCM)

The shrinking particle core model of the dissolution of mineral ores processes reaction is considered to take place first on the outer surface of material ore particles of interest. The porous zone penetrates into the solid particles and the particles shrink during the leaching process. The kinetics of the leaching process involves three sub-processes that occur during leaching:

i. The external diffusion of acid to the solid surface,
ii. Internal diffusion in the porous layer from the solution to the core surface and vice versa,
iii. Leaching reaction on the core surface. The rate of leaching (dissolution) is generally controlled diffusion through the porous layer or the dissolution reaction at the mineral surface of un-reacted particles [24]. One major factor that can affect interpretation of leaching data is the particle size distribution of a solid material. It was observed that the initial rate of leaching increased due to increase in the small particle fraction. The leaching process can also be described based on the residual volume of particles as shown in equation 1.

$$X(t) = 1 - \left[\frac{r(t)}{r_0}\right]^3 \quad (1)$$

Where: X(t) is the conversion rate, r(t) is the volume of unreacted core and r_o is the total volume of particle.

The rate of leaching is related to the surface area of solid particles [25]. The rate of leaching is a function of the surface area of the material to be analyzed. The primary hypothesis made in this study was that the increase in the surface area of leached ore particles was directly proportional to the increase in the tantalum content of the ore particles during the initial dissolution period.

Table 1. Response surface methodology design matrix for dissolution of tantalite mineral

Factor	Name	Units	Minimum	Maximum	Coded Low	Coded High
A	HF	M	1.0000	8.00	-1 ↔ 1.00	+1 ↔ 8.00
B	H_2SO_4	M	0.5000	3.00	-1 ↔ 0.50	+1 ↔ 3.00
C	TEMPERATURE	^0C	32.00	82.00	-1 ↔ 32.00	+1 ↔ 82.00
D	STIRRING SPEED	Rpm	0.0000	500.00	-1 ↔ 0.00	+1 ↔ 500.00
E	PARTICLE DIAMETERS	mm	0.1000	0.3000	-1 ↔ 0.10	+1 ↔ 0.30

2.1.4 Dissolution procedure

Following the response surface model design, sieved pulverized tantalite samples of particle diameter 0.1-0.3 mm were used for this experiment at different concentrations of hydrofluoric-sulphuric acid (1-8 M hydrofluoric and 0.5-3.0 M sulphuric acids) at a constant contact time of 240 minutes, stirring speed (between 0-500 rpm) and temperature (between 32^{o}C- 82^{o}C). The magnetic stirrer was introduced into the water bath and then 50 ml of the acids solution containing the pulverized sized tantalite ore (2 g) was placed inside the bath. The temperature and stirring speed was set and allowed to run. After run was completed the solution was taken out of the water bath, decanted and the residual tantalite ore was washed with distilled-deionized water and then transferred into a pre-weighed glass crucible. The crucible was placed in the oven and dried at 60^{o}C for about 2 hours and then reweighed. The weight of the residual tantalite ore and crucible was measured. The difference in weight was noted as the amount of tantalite ore undissolved. The percentage of the tantalite ore dissolved was calculated therefrom. The same procedure was repeated for all 50 runs from the experimental response surface design [26].

3. RESULTS AND DISCUSSION

The results of the elemental, oxide composition and mineral analysis into the composition of the material from the Okpella sample are shown in Tables 2 and 3. The result revealed high percentage of tantalum (34.17%), iron (12.55%), niobium (8.38%), and titanium (6.01%). Percentage of others elements are less than 5. Their oxides were also observed which exhibited a similar trend. Elements likethorium and tungsten exist as impurities in the ore sample and their presence could be used to design a separation method for their extraction and applications for radioactive purposes based on their economic values.

Table 3 and Fig. 1 shows the crystalline and peaks structure of this ore sample whose chemical composition is dominated by Ta, Fe, Ti, Nb, Mg, and Si indicates ore mineral constituents of a mixture of tantalite [(Ta, Nb)O_2], ilmenite ($FeTiO_3$) , Pyrite (Fe,Mn)S and Quartz (SiO_2). The niobium and Manganese, by their respective affinity for tantalum and iron are probably incorporated into the tantalite and pyrite phases respectively based on their chemistry. The ilmenite, pyrite and quartz gives information on the reducing conditions of formation of the ore while the thorium value points to its lithosphere origin according to Baba et al. [27]. Okunlola [28], stated that tantalite ore could be radioactive by virtue of its very low thorium and tungsten content, suggesting why some Ta/Nb minerals cannot be shipped out of the country, because of their levels of radioactivity on the limits of allowed thorium (0.08%) and tungsten (0.15%) contents. The X – ray diffraction spectrum show tantalite characteristic diffraction peaks at 2.56 A^{o}, 2.39 A^{o}, 1.76 A^{o}, 1.50 A^{o} and 1.43 A^{o}.

Table 2. Characterization of tantalite ore percentage elements and their oxides from XRF analysis

S/N	Element	% Element	% Oxide	% Oxide
1	Si	2.180	SiO_2	4.660
2	Al	0.800	Al_2O_3	1.520
3	Ta	34.170	Ta_2O_5	41.720
4	Ca	0.310	CaO	0.430
5	Fe	12.550	Fe_2O_3	17.940
6	Mg	3.620	MgO	6.000
7	K	0.007	K_2O	0.090
8	Cr	0.027	Cr_2O_3	0.040
9	Na	0.015	Na_2O	0.020
10	P	0.013	P_2O_5	0.030
11	Sn	0.134	SnO_2	0.170
12	Mn	1.738	MnO_2	2.750
13	Ti	6.006	TiO_2	10.020
14	Nb	8.375	Nb_2O_5	11.980
15	W	0.119	WO_3	0.150
16	Th	0.066	ThO_3	0.080

Table 3. Results of XRD characterization of tantalite ore

Peak	2Θ/degree	Plane	Minerals	Compositions (wt%)
1	23.00	110	Quartz	3.92
2	24.89	101	Quartz	6.36
3	32.93	111	Ilmenite	12.68
4	35.02	020	Tantalite/Quartz	11.73
5	37.60	121	Tantalite	38.47
6	42.50	211	Pyrite	7.70
7	48.53	202	Ilmenite	3.55
8	52.00	123	Tantalite	3.20
9	55.24	232	Pyrite	4.35
10	62.00	331	Tantalite	3.28
11	65.08	152	Tantalite	4.74

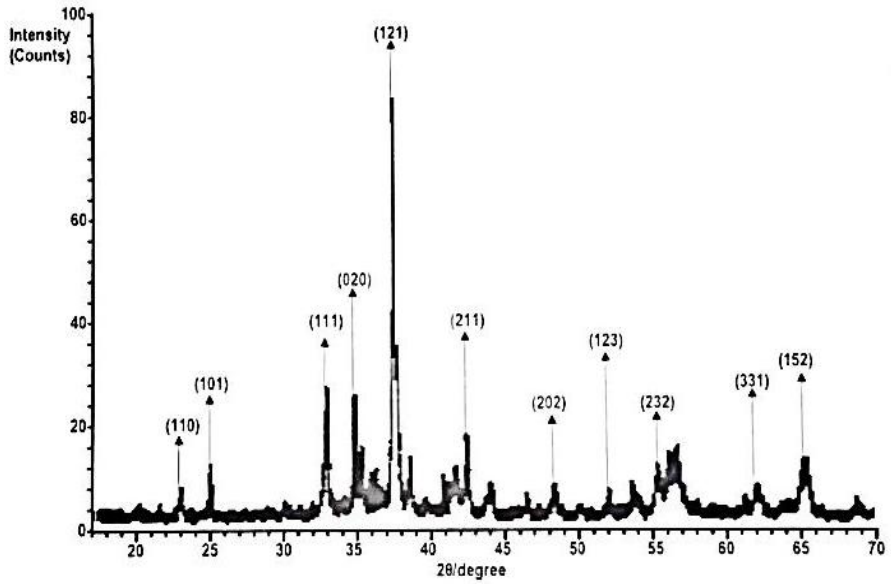

Fig. 1. XRD characteristic peaks of tantalite ore

3.1 The Experimental Dissolution Runs for Tantalite Mineral Sample

Tantalite ore underwent 50 dissolution experiments detailed in Table 4, where varying concentrations of acids, temperatures, stirring speeds, and particle sizes were employed to optimize the dissolution conditions. The percentage of dissolution observed across these experiments is tabulated in Table 4. Among these, run 2 demonstrated the highest dissolution percentage, likely due to the combination of high HF concentration (8 M) and low H_2SO_4 concentration (0.5 M), elevated dissolution temperature (82°C), rapid stirring (500 rpm), and larger particle diameter (0.1 mm) of the tantalite ore. These conditions highlight significant potential for enhancing leaching efficiency in tantalite ore. The dissolution behavior observed aligns with findings reported by Baba et al. [9]. Increasing HF concentration accelerates the reaction rate of the tantalite-HF solution by promoting molecular collisions, consistent with Le Chatelier's principle, which favors dissolution equilibrium. Experimental results indicate that an 8 M HF concentration notably influences the leaching process of the mineral core. The complementary role of 0.5 M H_2SO_4 is also evident, aiding in dissolving impurities such as carbonates or silicates found in tantalite minerals. This dissolution exposes a greater surface area of tantalite to HF, facilitating faster attack. Furthermore, H_2SO_4 enhances the solution's ionic strength and stabilizes pH, preventing salting out that may arise from the dissolution of mineral gangue components like carbonates and silicates.

Table 4. Response of % Solubility at different Variable Factors and Shrinking Sphere of Tantalite Ore

	Factor 1	Factor 2	Factor 3	Factor 4	Factor 5	Response 1	Response 2	Conversion time expression for Shrinking sphere (Shrinking core model)	
Run	A:HF	B:H_2SO_4	C:TEMPERATURE	D:STIRRING SPEED	E:PARTICLE DIAMETERS	SOLUBILIY	PREDICTED		
	Conc.	Conc.	ºC	Rpm	Mm	%	%	Film diffusion control ($t/\tau = 1-(1-X_B)^{2/3}$)	Reaction controls ($t/\tau = 1-(1-X_B)^{1/3}$)
1	4.5	1.75	57	250	0.2	66.58	58.47	0.888	0.666
2	**8**	**0.5**	**82**	**500**	**0.1**	**97.28**	**88.75**	**0.999**	**0.973**
3	5	2.25	67	300	0.2	68.5	62.05	0.901	0.685
4	8	3	32	500	0.1	84.87	81.20	0.977	0.849
5	1	3	82	350	0.1	48.76	40.80	0.737	0.488
6	8	0.5	82	400	0.3	87.42	85.08	0.984	0.874
7	6	1.5	57	150	0.2	53.84	64.79	0.787	0.538
8	7	3	82	100	0.1	68.38	67.91	0.900	0.684
9	8	1	67	300	0.3	80.84	80.76	0.963	0.808
10	1	2	82	500	0.1	45.98	46.65	0.708	0.460
11	3	3	57	250	0.2	51.83	47.59	0.768	0.518
12	4.5	2.25	42	300	0.2	54.96	57.99	0.797	0.550
13	5	1	72	200	0.2	57.43	62.24	0.819	0.574
14	8	0.5	32	150	0.1	79.63	77.24	0.959	0.796
15	8	3	82	500	0.3	75.11	82.64	0.938	0.751
16	1	0.5	82	5003	0.3	46.82	48.55	0.717	0.468
17	8	0.5	32	400	0.1	85.73	83.64	0.980	0.857
18	4	3	67	350	0.1	52.78	56.80	0.777	0.528
19	6	0.5	57	250	0.2	63.75	69.35	0.869	0.638
20	8	0.5	82	500	0.2	93.89	88.20	0.996	0.939
21	3	1	42	250	0.2	49.87	50.83	0.749	0.499
22	1	0.5	32	500	0.1	48.36	47.11	0.733	0.484
23	2	2.25	57	250	0.2	43.29	43.50	0.678	0.4329
24	1	0.5	82	500	0.1	42.77	49.65	0.672	0.428
25	8	3	32	450	0.3	87.72	78.82	0.985	0.877
26	6	1.75	57	300	0.2	62.84	68.13	0.862	0.628
27	7	1.75	57	250	0.2	67.54	72.43	0.895	0.675
28	8	3	32	0	0.1	72.36	68.39	0.924	0.724

	Factor 1	Factor 2	Factor 3	Factor 4	Factor 5	Response 1	Response 2	Conversion time expression for Shrinking sphere (Shrinking core model)	
Run	A:HF	$B:H_2SO_4$	C:TEMPERATURE	D:STIRRING SPEED	E:PARTICLE DIAMETERS	SOLUBILIY	PREDICTED		
	Conc.	Conc.	ºC	Rpm	Mm	%	%	Film diffusion control ($t/\tau = 1-(1-X_B)^{2/3}$)	Reaction controls ($t/\tau = 1-(1-X_B)^{1/3}$)
29	4	2	42	250	0.2	56.94	54.41	0.815	0.569
30	6	3	82	500	0.1	68.56	72.57	0.901	0.686
31	5	3	32	0	0.1	43.22	51.64	0.678	0.432
32	2	0.5	82	250	0.2	48.17	48.28	0.731	0.482
33	1	1	67	400	0.1	41.33	45.32	0.656	0.413
34	3	2	82	0	0.3	45.25	43.91	0.700	0.453
35	4	0.5	82	500	0.3	63.72	65.30	0.868	0.637
36	7	0.5	32	0	0.3	68.88	66.71	0.903	0.689
37	6	0.5	82	0	0.1	71.56	64.77	0.919	0.716
38	2	1.75	57	250	0.2	52.95	44.51	0.779	0.530
39	5	1.75	57	250	0.2	64.29	61.26	0.872	0.643
40	8	2	42	250	0.2	74.89	76.76	0.937	0.749
41	3	0.5	67	350	0.3	52.62	55.11	0.776	0.526
42	4	2	32	250	0.2	54.77	53.90	0.795	0.548
43	5	3	32	0	0.3	44.58	50.53	0.693	0.446
44	1	3	32	500	0.3	41.82	41.00	0.662	0.418
45	1	0.5	82	0	0.3	40.76	35.74	0.649	0.408
46	1	0.5	32	0	0.3	38.63	33.19	0.623	0.386
47	5	1	57	250	0.2	46.95	62.76	0.719	0.470
48	8	3	82	0	0.3	70.95	69.83	0.916	0.710
49	7	0.5	32	0	0.1	65.76	67.81	0.883	0.658
50	8	0.5	32	200	0.3	76.55	77.42	0.945	0.766

Table 5. Analysis of Variance and Significance for Tantalite Dissolution Regression Model

Source	Sum of Squares	Df	Mean Square	F-value	p-value	
Model	10912.78	20	545.64	16.70	< 0.0001	Significant
A-HF	5306.94	1	5306.94	162.40	< 0.0001	
B-H2SO4	106.76	1	106.76	3.27	0.0811	
C-TEMPERATURE	45.48	1	45.48	1.39	0.2477	

Source	Sum of Squares	Df	Mean Square	F-value	p-value
D-STIRRING SPEED	465.97	1	465.97	14.26	0.0007
E-PARTICLE DIAMETERS	19.23	1	19.23	0.5885	0.4492
AB	49.66	1	49.66	1.52	0.2276
AC	0.4573	1	0.4573	0.0140	0.9067
AD	48.24	1	48.24	1.48	0.2342
AE	5.28	1	5.28	0.1616	0.6906
BC	0.3600	1	0.3600	0.0110	0.9171
BD	6.03	1	6.03	0.1845	0.6707
BE	10.64	1	10.64	0.3257	0.5726
CD	68.49	1	68.49	2.10	0.1584
CE	25.38	1	25.38	0.7766	0.3854
DE	8.76	1	8.76	0.2679	0.6087
A^2	113.52	1	113.52	3.47	0.0725
B^2	2.01	1	2.01	0.0614	0.8060
C^2	18.85	1	18.85	0.5770	0.4536
D^2	1.67	1	1.67	0.0511	0.8227
E^2	8.64	1	8.64	0.2643	0.6111
Residual	947.66	29	32.68		
Cor Total	11860.44	49			
R^2	0.9201				
Adjusted R^2	0.8650				
Predicted R^2	0.6560				
Adeq Precision	15.0622				

The optimization model for tantalite dissolution underwent significance analysis and testing (Table 5). The regression model yielded an F-value of 16.70 with a P-value of 0.0001, significantly less than 0.0500, indicating high significance of the tantalite dissolution model. The absence of misfit for the F-value and R-value suggests the model's overall significance. Consequently, it serves as a reliable predictor of the effects of acid concentrations HF (A) and H_2SO_4 (B), temperature (C), stirring speed (D) and particle diameters (E) on tantalite dissolution across the investigated regression range. P-values for variables A and D are ≤ 0.05, indicating their profound and significant influence on tantalite dissolution, while those for B, C, and E exceed 0.05. Terms A^2, CD, AB, AD, C, CE, E, C^2, BE, DE, E^2, BD, AE, B^2, D^2, AC, and BC have P-values > 0.1000, suggesting potential for model refinement through reduction. Based on F-values, the order of significance among influencing factors is A > D > B > A^2 > CD > AB > AD > C > CE > E > C^2 > BE > DE > E^2 > BD > AE > B^2 > D^2 > AC > BC. The R^2 value of 0.9201 for the linear model of tantalite ore dissolution into mixed acid confirms a robust quadratic equation model [28]. An adjusted R^2 of 0.8650 falls within a satisfactory range, with predicted R^2 values at 0.6560. The difference between adjusted and predicted R^2 values (< 0.2000) is acceptable [29,30]. The Adequate Precision value of 15.0622, indicating a satisfactory signal-to-noise ratio, supports the model's suitability for predicting tantalite ore dissolution and tantalum recovery [29].

3.2 Final Equation in Terms of Coded and Actual Factors

Coded equation: % dissolution of tantalite ore = 55.95 + 18.25*A – 2.10*B + 1.35*C + 5.42*D – 0.9348*E – 1.83*AB – 0.1948*AC + 2.62*AD – 0.6292*AE + 0.1717*BC – 0.7807*BD – 0.7528*BE – 2.35*CD – 1.29*CE + 0.9470*DE + 4.77*A^2 – 0.7096*B^2 + 2.64*C^2 + 0.9810*D^2 – 1.66*E^2 (2)

Actual equation: % dissolution of tantalite ore = 29.23375 + 2.17969 A – 3.30489B - 0.230317C + 0.018598D + 95.74283E – 0.417245AB – 0.002226AC + 0.002995AD – 1.79775AE + 0.005495BC – 0.002498BD – 6.02262BE – 0.000376CD – 0.515512CE + 0.037879DE + 0.389314A^2 – 0.454116B^2 + 0.004229C^2 + 0.000016D^2 – 166.36807E^2 (3)

The equation in terms of coded factors allows predictions of the response at specified levels of each factor. In this coding scheme, high levels of factors are denoted as +1 and low levels as -1. This coded equation facilitates comparing the coefficients of factors to assess their relative impact. Conversely, the equation in terms of actual factors predicts the response based on specific levels of each factor in their original units. Unlike the coded equation, this form should not be used to determine the relative impact of factors because the coefficients are adjusted to account for the units of each factor, and the intercept does not align with the center of the design space.

In Fig. 2(a), the model-predicted dissolution of tantalite ore was compared with the actual dissolution rate, revealing that the actual values closely follow a linear trend. Fig. 2(b) demonstrates that the residuals between tantalite ore values and their predictions fall within acceptable limits. Thus, the response surface method used to model tantalite ore dissolution proves reliable across the entire range of regression.

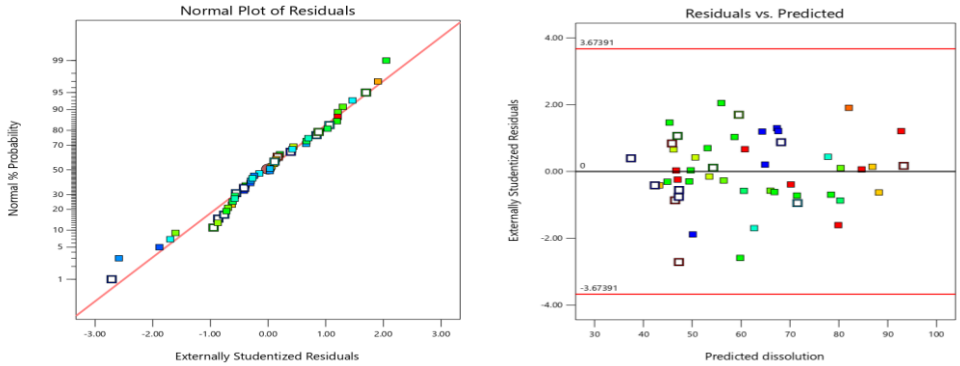

2a 2b

Fig. 2. Relation between Predicted and Actual Dissolution of Tantalite Ore (a). Predicted vs Actual Dissolution: (b). Residual and Predicted Dissolution Distribution

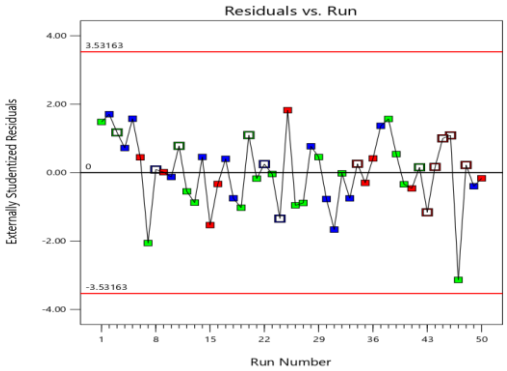

Fig. 3. Probability Plot of Externally Studentized Residuals vs Run Number for Dissolution of Tantalite Ore

The externally studentized residuals in the dissolution of tantalite ore serve as a statistical tool to evaluate the normality of residuals and detect potential outliers within a linear regression model. This approach, applied to predict tantalite ore dissolution, yielded significant results, as evidenced by values presented in Table 6 for model comparison and fit statistics. The model's confidence level was established at 95%. The strong relationship observed between R-squared and Adjusted R-squared underscores the model's robustness. However, a low Predicted R-squared suggests that the mean could be a more effective predictor than the current model. In some instances, employing a higher-order model may enhance predictive accuracy. Adequate precision, as defined by the signal-to-noise ratio (Adeq Precision), is crucial. A ratio exceeding 4 is desirable, and in this case, a ratio of 15.0622 indicates a satisfactory signal, affirming the model's utility in navigating the design space [30,31].

Table 6. Model comparison and fit statistics for tantalite ore dissolution

Model Comparison Statistics		Fit Statistics	
PRESS	4079.64	Std Dev.	5.72
-2 Log Likelihood	288.99	Mean	61.45
BIC	371.14	C.V.%	9.30
AICc	363.99	R^2	0.9201
		Adjusted R^2	0.8650
		Predicted R^2	0.6560
		Adeq Precision	15.0622

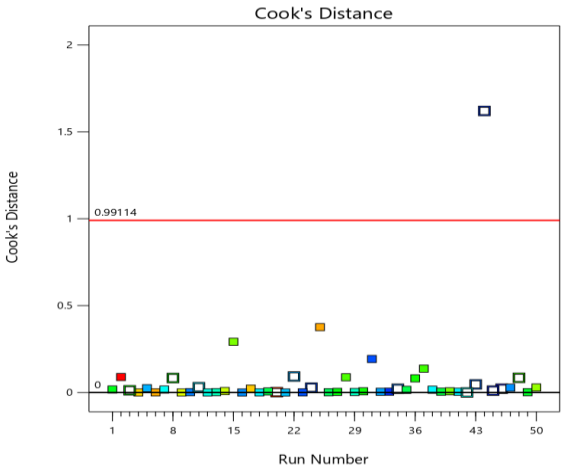

Fig. 4. Plot of Cook's Distance vs Run Number

Fig. 4 The Cook's distance plot, highlighting a particular data point that appears to exert significant influence owing to its position within the factor. Based on this observation, it is determined that the empirical model adequately characterizes tantalite dissolution in the HF-H_2SO_4 medium [31].

Fig. 5(a) displays leverage versus run number, indicating that only one run exhibits a high leverage value, which may not significantly affect the model. All runs in this figure are precisely fitted with only one residual and show no instances of high leverage [32].

Fig. 5(b) presents the difference in fits (DFFITS) graph, where a substantial number of observations have positive DFFITS values. Notably, the predicted value at observation 2 is higher when included in the model compared to when excluded, indicating that these observations elevate the regression. Conversely, twenty-three observations show large negative DFFITS values, suggesting they depress the regression and exert influence on the fitted values [33].

Fig. 5(c) depicts the difference in beta values (DFBETAS) for intercept plot, revealing that several points exert significant influence on the slope estimate for tantalite ore dissolution in HF-H_2SO_4 medium. Some points diverge from the primary linear trend, suggesting they follow a distinct data-generating process influenced by varying factors [34,35].

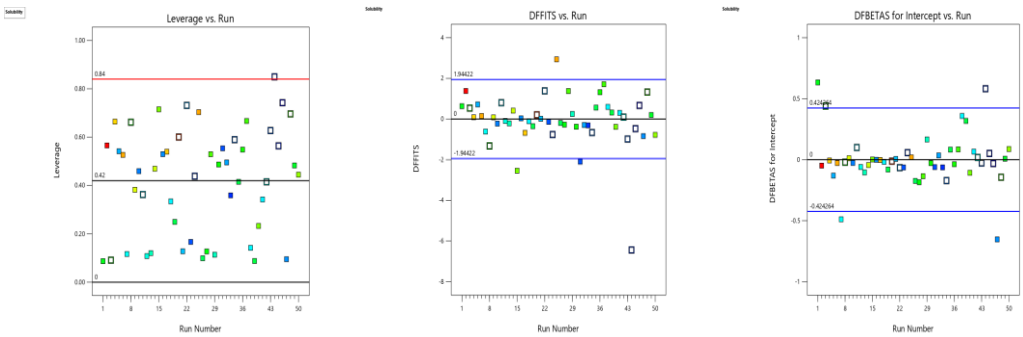

Fig. 5. (a)Leverage vs Run Number Plot, (b) DFFITS vs Run Number Plot, and (c)DFBETAS for Intercept vs Run Number Plot

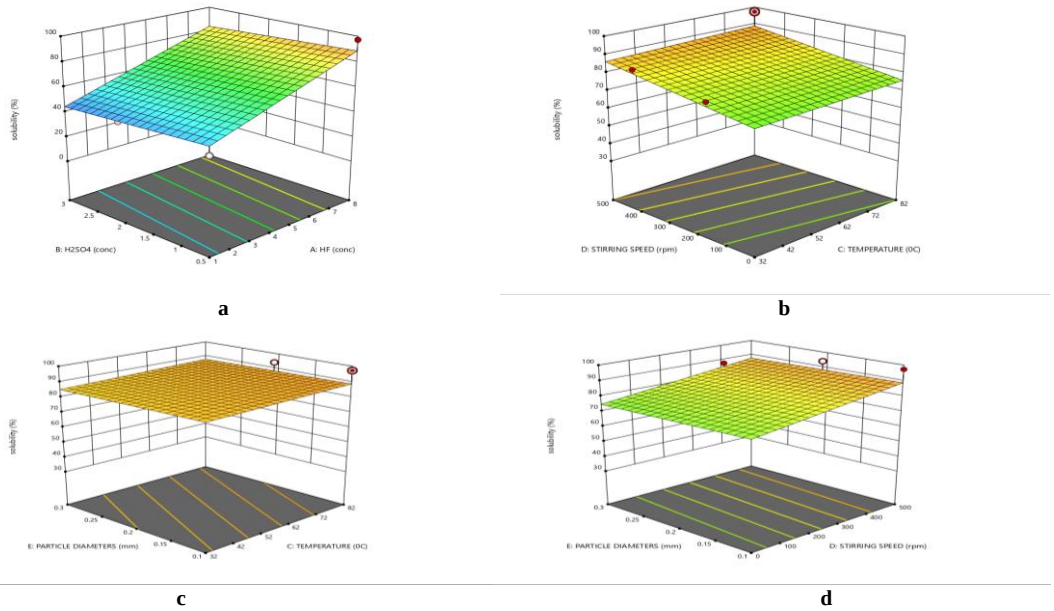

Fig. 6. Response Surface Methodology Plots for the Interactions between the Dissolution Factors and the Percentage Tantalite Leached. (a= mixed acid HF and H_2SO_4) (b= (stirring speed and temperature) (c=particle diameters and temperature) (d=particle diameters and stirring speed)

The study investigated interactions among factors A (HF concentration) and B (H_2SO_4 concentration), factor C (temperature), factor D (stirring speed), and factor E (particle size) to understand their combined effects on the leaching of tantalite ore. Response surface methodology (RSM) facilitated the creation of 3D response surfaces, with optimal conditions indicated by convergence in dark red areas, signifying maximum tantalite ore leaching [28].

Fig. 6(a, b, c, and d) presents RSM 3D plots based on actual model equations (1 and 2) for percentage tantalite ore leached. Notably, percentage dissolution improved with higher HF concentration (1-8 M) and lower H_2SO_4 concentration (0.5-3 M) (Fig. 6a). According to Yang et al. [36], Li et al. [37], and Harrar et al. [38], increased acid load increases hydronium ion concentration, lowering pH near zero, while lower sulfuric acid concentration aids gangue mineral dissolution and maintains solution acidity, promoting fluorotantalate complex formation.

The RSM 3D plot for tantalite ore dissolution also considered simultaneous effects of leaching temperature (320°C to 820°C) and stirring speed (0 to 500 rpm), revealing increased dissolution (up to 97.28%) at higher temperatures and speeds. Elevated temperature and speed enhance molecular motion and collisions, reducing the boundary layer around ore particles, favoring acid contact (Fig. 6b).

Fig. 6(a) highlights critical factors influencing tantalite ore dissolution, with temperature and stirring speed exerting more pronounced effects than acid concentration and particle size, as evidenced by contour line distribution. Figure 6(b) emphasizes the importance of particle size and temperature, with finer particles providing increased surface area for acid contact and reduced travel distance for acid molecules to reach unreacted tantalum within the ore.

The developed 3D surface response models offer insights for optimizing tantalite ore dissolution. Optimal operating parameters identified include HF concentration of 8 M, H_2SO_4 concentration of 0.5 M, temperature of 82°C, stirring speed of 500 rpm, and particle size of 0.1 mm, which significantly enhance tantalite dissolution efficiency.

3.3 Desirability Function for Optimal Dissolution Parameters

The optimal dissolution conditions for tantalite ore were identified through Design of Experiment, as outlined in Table 3. A desirability function was utilized to maximize the percentage of tantalite dissolution by optimizing variables A (HF concentration), B (H_2SO_4 concentration), C (Temperature), D (Stirring speed), and E (Particle diameter). Table 7 presents the parameter configurations that achieve the desired target response.

The desirability function operates within the range of (0, 1), where a value of 1 signifies maximum satisfaction and 0 indicates an unacceptable or undesirable response [39]. Table 7 illustrates that in this design, runs 28 from Table 8 was selected as optimal for tantalite dissolution of 88.75%, achieving the highest percentage dissolution. Furthermore, runs 28 achieved a desirability score of 1.0, indicating maximum satisfaction with the chosen conditions. The optimal dissolution conditions for tantalite ore involve HF and H_2SO_4 concentrations of 8 M and 0.5 M respectively, a temperature of 82°C, a stirring speed of 500 rpm, and a particle size of 0.1 mm.

Table 8 is the initial total number of runs given by the design expert which was later resolve to the 50 experimental run (Table 4).

Table 7. Dissolution parameters setting for the optimal response of Tantalite ore

Name	Goal	Lower Limit	Upper Limit
A:HF	is in range	1	8
B:H_2SO_4	is in range	0.5	3
C:TEMPERATURE	is in range	32	82
D:STIRRING SPEED	is in range	0	500
E:PARTICLE DIAMETERS	is in range	0.1	0.3
Solubility	Maximize	38.63	97.28

Table 8. Dissolution conditions of the optimized solutions for tantalite ore

Number	HF	H_2SO_4	Temperature	Stirring Speed	Particle Diameters	Solubility	Desirability	
1	4.724	1.737	47.688	195.410	0.292	57.365	1.000	
2	5.000	1.000	57.000	250.000	0.200	62.763	1.000	
3	5.000	1.000	72.000	200.000	0.200	62.244	1.000	
4	1.000	3.000	32.000	500.000	0.300	41.001	1.000	
5	7.000	0.500	32.000	0.000	0.300	66.707	1.000	
6	7.000	3.000	82.000	100.000	0.100	67.911	1.000	
7	8.000	3.000	82.000	500.000	0.300	82.643	1.000	
8	8.000	0.500	82.000	500.000	0.200	88.197	1.000	
9	5.000	3.000	32.000	0.000	0.300	50.533	1.000	
10	4.500	1.750	57.000	250.000	0.200	58.469	1.000	
11	2.000	2.250	57.000	250.000	0.200	43.505	1.000	
12	8.000	0.500	32.000	400.000	0.100	83.644	1.000	
13	1.000	2.000	82.000	500.000	0.100	46.647	1.000	
14	7.000	0.500	32.000	0.000	0.100	67.809	1.000	
15	8.000	3.000	32.000	0.000	0.100	68.392	1.000	
16	2.000	1.750	57.000	250.000	0.200	44.505	1.000	
17	5.000	3.000	32.000	0.000	0.100	51.635	1.000	
18	8.000	3.000	82.000	0.000	0.300	69.832	1.000	
19	8.000	0.500	82.000	400.000	0.300	85.083	1.000	
20	4.500	2.250	42.000	300.000	0.200	57.987	1.000	
21	6.000	3.000	82.000	500.000	0.100	72.574	1.000	
22	6.000	0.500	57.000	250.000	0.200	69.349	1.000	
23	8.000	1.000	67.000	300.000	0.300	80.758	1.000	
24	3.000	0.500	67.000	350.000	0.300	55.111	1.000	
25	1.000	0.500	82.000	0.000	0.300	35.735	1.000	
26	6.000	0.500	82.000	0.000	0.100	64.766	1.000	
27	3.000	1.000	42.000	250.000	0.200	50.829	1.000	
28	**8.000**	**0.500**	**82.000**	**500.000**	**0.100**	**88.748**	**1.000**	**Selected**
29	2.000	0.500	82.000	250.000	0.200	48.278	1.000	
30	4.000	3.000	67.000	350.000	0.100	56.797	1.000	
31	3.000	2.000	82.000	0.000	0.300	43.905	1.000	
32	4.000	2.000	42.000	250.000	0.200	54.413	1.000	
33	4.000	2.000	32.000	250.000	0.200	53.905	1.000	
34	1.000	0.500	82.000	500.000	0.300	48.546	1.000	
35	8.000	0.500	32.000	150.000	0.100	77.238	1.000	
36	1.000	0.500	32.000	500.000	0.100	47.106	1.000	

Number	HF	H_2SO_4	Temperature	Stirring Speed	Particle Diameters	Solubility	Desirability
37	1.000	0.500	82.000	500.000	0.100	49.649	1.000
38	6.000	1.500	57.000	150.000	0.200	64.786	1.000
39	1.000	3.000	82.000	350.000	0.100	40.803	1.000
40	1.000	0.500	32.000	0.000	0.300	33.193	1.000
41	3.000	3.000	57.000	250.000	0.200	47.589	1.000
42	8.000	3.000	32.000	500.000	0.100	81.203	1.000
43	5.000	2.250	67.000	300.000	0.200	62.051	1.000
44	8.000	2.000	42.000	250.000	0.200	76.756	1.000
45	8.000	3.000	32.000	450.000	0.300	78.819	1.000
46	1.000	1.000	67.000	400.000	0.100	45.323	1.000
47	8.000	0.500	32.000	200.000	0.300	77.417	1.000
48	4.000	0.500	82.000	500.000	0.300	65.303	1.000
49	5.000	1.750	57.000	250.000	0.200	61.262	1.000
50	6.000	1.750	57.000	300.000	0.200	68.129	1.000
51	1.229	1.265	58.920	488.792	0.164	47.586	1.000
52	4.140	1.509	36.696	199.874	0.129	55.016	1.000
53	5.701	2.893	68.748	294.590	0.258	64.311	1.000
54	2.760	1.135	64.171	459.291	0.190	55.762	1.000
55	2.965	1.037	77.870	44.194	0.254	46.812	1.000
56	7.025	1.397	53.067	417.968	0.171	77.541	1.000
57	3.669	2.442	75.447	215.477	0.134	52.860	1.000
58	4.994	0.919	71.174	244.671	0.197	63.493	1.000
59	6.589	2.616	53.149	325.866	0.173	70.304	1.000
60	2.228	1.121	80.934	121.923	0.186	45.049	1.000
61	5.082	1.427	73.971	70.871	0.298	58.103	1.000
62	6.421	1.113	63.905	104.296	0.153	67.354	1.000
63	6.984	2.346	32.614	162.465	0.169	67.843	1.000
64	2.025	2.074	70.371	443.553	0.120	50.074	1.000
65	7.432	2.874	63.369	269.924	0.190	73.485	1.000
66	4.799	2.025	33.337	287.553	0.218	59.250	1.000
67	4.047	2.671	39.699	167.814	0.236	50.914	1.000
68	6.536	1.890	60.711	243.723	0.208	69.544	1.000
69	3.403	2.016	80.058	423.466	0.172	57.582	1.000
70	5.175	2.236	52.172	160.680	0.267	58.366	1.000
71	6.193	1.903	33.973	80.403	0.224	61.970	1.000
72	6.774	2.442	61.230	213.113	0.281	68.613	1.000
73	1.400	2.494	64.405	148.295	0.150	37.711	1.000
74	3.454	0.851	81.242	150.803	0.194	53.149	1.000

Number	HF	H_2SO_4	Temperature	Stirring Speed	Particle Diameters	Solubility	Desirability
75	4.153	0.726	73.352	238.515	0.279	58.679	1.000
76	7.523	1.358	80.358	367.817	0.172	80.496	1.000
77	3.249	1.176	64.203	403.902	0.289	56.448	1.000
78	1.021	0.836	47.873	114.362	0.152	37.195	1.000
79	7.063	2.012	72.768	340.269	0.186	75.453	1.000
80	3.778	2.704	64.940	237.556	0.180	52.723	1.000
81	3.022	1.056	38.270	80.687	0.124	46.734	1.000
82	6.071	2.221	67.927	270.428	0.164	67.581	1.000
83	2.319	2.220	75.650	367.923	0.211	49.255	1.000
84	3.794	2.240	63.687	153.378	0.163	51.612	1.000
85	4.236	2.997	80.699	417.997	0.100	60.558	1.000
86	1.268	1.882	52.747	224.111	0.253	38.980	1.000
87	7.652	1.685	72.767	7.368	0.161	71.004	1.000
88	3.884	1.159	58.347	135.066	0.154	53.592	1.000
89	6.537	2.133	49.266	135.270	0.103	66.284	1.000
90	3.167	2.843	62.348	490.644	0.199	55.280	1.000
91	1.292	1.850	44.253	368.856	0.183	42.839	1.000
92	7.005	0.795	58.963	479.065	0.254	80.041	1.000
93	4.081	0.738	34.169	387.459	0.251	60.232	1.000
94	7.464	1.018	49.986	298.226	0.136	77.723	1.000
95	7.089	1.663	45.583	389.823	0.246	75.852	1.000
96	5.817	1.801	63.713	428.055	0.136	70.979	1.000
97	1.017	2.011	74.390	431.834	0.135	44.393	1.000
98	7.904	1.543	48.730	119.589	0.293	73.618	1.000
99	5.179	1.032	80.940	150.226	0.198	62.372	1.000
100	1.788	1.506	56.870	372.842	0.200	46.949	1.000

The predicted optimized percentage tantalite ore dissolution model equations 2-3 and conditions were within a 95% confidence level (Table 9). Moreover, the point prediction provided a standard deviation of 5.72 (Table 9). This implies that the predicted and experimental percentage dissolution of the tantalite ore from the optimized dissolution conditions (Table 9) will not deviate by more than 6% for the sample. The predicted percentage tantalite ore dissolution mean and median is 92.76 (Table 9). This value is close to the expected dissolved tantalite ore for the optimized dissolution condition, illustrating the model's accuracy in the optimized dissolution conditions.

Based on the validated model, tantalite ore was dissolved under the achieved optimal conditions: HF and H_2SO_4 concentrations of 8 M and 0.5 M respectively, a stirring speed of 500 rpm, particle size of 0.1 mm, and a dissolution temperature of 82°C. Under these conditions, the experimental dissolution percentage of tantalite ore was 97.28%, whereas the predicted dissolution percentage was 88.75% (refer to Table 3). The percentage of absolute error (POAE) was calculated using the equation 4.

$$\text{POAE} = \frac{experimental\,\%\,dissolution - predicted\,\%\,dissolution}{experimental\,\%\,dissolution}\,x\,100 \quad (4)$$

The error percentage for tantalite ore dissolution under optimal conditions was 4.65%. According to Ajemba and Onukwuli [40], the generally accepted range for percentage of absolute error (POAE) should typically fall between 2.50% and 5.00%, depending on the nature of the experiment. The achieved POAE indicates that the optimized outcomes and findings align satisfactorily with the experimental results.

3.4 Dissolution Kinetics Using Shrinking Core Model (SCM)

To establish the reaction kinetics and rate controlling step for the dissolution of tantalite in HF-H_2SO_4, the experimental data were analyzed using the shrinking core model (SCM). The fluid-solid heterogeneous reaction can be represented in the form as equation 5

$$\underset{\text{Reactants}}{X\,(aq) + yY\,(s)} \longrightarrow \text{Products} \quad (5)$$

From the shrinking core model, the reaction is considered to take place first at the outer surface of the particle [41]. The region of the reaction goes into the solid and the reacting particle shrinks during the reaction. The reactions occurring in the fluid-solid heterogeneous system generally have the following steps:

- ✓ Diffusion of fluid reactant through the main body of the fluid layer to the surface of the solid.
- ✓ Reaction of the fluid reactant with the solid on the surface of the solid.
- ✓ Diffusion of the products through the film layer back to the bulk of the fluid.

The slowest of these steps is considered the rate determining step using the stokes regime (small particles). The rate may be described by film diffusion, chemical reaction, or product layer diffusion models. The rate equations can be written as equation 6 and 7

Table 9. Point Prediction table for the optimized selected solutions

Run 2 Response	Predicted Mean	Predicted Median	Observed	Std Dev	SE Mean	95% CI low for Mean	95% CI high for Mean
Solubility	92.7581	92.7581	97.2800	5.71646	4.29947	83.9647	101.5520

Std Dev: Standard Deviation; CI: Confidence Level Two-sided Confidence = 95% Population = 99%

$$\frac{t}{\tau} = 1 - (1 - X_B)^{2/3}$$

$$\tau = \frac{\rho_B R_0^2}{2b\mathscr{D}C_{Ag}} \quad \text{(The film diffusion equation)} \quad (6)$$

Where t/τ is the contact time or reaction time needed for any specific conversion of solid in the plug flow, X_B is the conversion, τ is the time for complete conversion of a particle which is the rate constant, ρ_B is the molar density of the solid, R is the original cylindrical pellet, C_{Ag} is concentration in the gas phase, $\mathscr{D}$ is the volume.

$$\frac{t}{\tau} = 1 - (1 - X_B)^{1/3}$$

$$\tau = \frac{\rho_B R_0}{bk'' C_{Ag}} \quad \text{(The reaction control equation)} \quad (7)$$

Where t/ τ is the contact time or reaction time needed for any specific conversion of solid in the plug flow, X_B is the conversion, τ is the time for complete conversion of a particle which is the rate constant, ρ_B is the molar density of the solid, R is the original cylindrical pellet, C_{Ag} is concentration in the gas phase, K" is the e mass transfer coefficient between fluid and particle.

The analysis of the experimental data using the above equations showed that the dissolution of Okpella tantalite in hydrofluoric-sulphuric acid solution is controlled by Stokes Regime (Small Particles). At the time when a particle, originally of size R_o has shrunk to size R, we may write:

$$t = \frac{\rho_B R_0^2}{2bC_{Ag}\mathscr{D}}\left[1 - \left(\frac{R}{R_0}\right)^2\right] \quad (8)$$

The time for complete disappearance of a particle is thus

$$\tau = \frac{\rho_B R_0^2}{2bC_{Ag}\mathscr{D}} \quad (9)$$

and on combining equation 8 and 9 gives equation 10

$$\frac{t}{\tau} = 1 - \left(\frac{R}{R_0}\right)^2 = 1 - (1 - X_B)^{2/3} \quad (10)$$

3.5 Effect of Variable Factors

The evaluation of the effect of variable factors (acid concentration, temperature, stirring speed and particle diameters) conducted on tantalite dissolution has been reported from the results as illustrated in Table 4. As the concentration of HF acid increases; decrease in the H_2SO_4; increase in temperature; increase in stirring speed and increase in surface area via reduction in particle sizes, the dissolution process increases as a result of constant interaction of the solution and the particle of the tantalite mineral affecting the rate of the leaching process, i.e., both the diffusion and the reaction rate [42]. The results of this experiment as presented in Table 4 do explain the leaching process of the reaction. Leaching is a heterogeneous reaction between solid particles and a liquid [43]. In the case of studying the dissolution rate of tantalite in acid solution (HF-H_2SO_4), the reaction(s) took place at the interface of tantalite (solid phase) and acids (liquid) and the leaching reaction could be expressed as follows:

$$\underset{\text{Reactants}}{HF + H_2SO_4 + (Fe, Mn)(Ta, Nb)_2O_6} \longrightarrow \text{Products} \quad (11)$$

Generally, during leaching, the following sequence of events occurs: the diffusion of the leaching agent (Hydrofluoric – sulphuric acid mix) through a thin liquid film surrounding the tantalite particles; anodic and cathodic reactions occur on the surface of the tantalite particles (including charge transfer); then, the diffusion of the produced products, i.e., Ta^{5+}, Nb^{5+}, Fe^{2+}, Mn^{2+}, F^-, H^+, SO_4^{2-}, and XH_2O into the bulk solution takes place. The slowest process acts as a limiting step and controls the kinetic model [43].

To determine the kinetics of tantalite dissolution in hydrofluoric-sulphuric acid mix and other parameters variation, experimental results of the studied parameters were evaluated using the new equation proposed by Dickinson and Heal, [44]. In the shrinking core model. Further references indicated below provide additional confirmation of our choice. The Dickinson and Heal [38] model defines the interfacial transfer and diffusion (mixed model) through the product as equation 12 ($t/\tau = 1-(1-X_B)^{2/3}$; ($t/\tau = 1-(1-X_B)^{1/3}$), Here, X is the fractional conversion, t is time (min), and τ is the rate constant (min^{-1}) [45-47]. Thus, the mechanism of tantalite dissolution in hydrofluoric-sulphuric acid mix occurs, which consists of anodic and cathodic reactions occurring at the tantalite–solution surface (interfacial layer); then, the movement of the produced ionic species diffuses into the bulk solution and can be kinetically described by the values obtained from the film diffusion control and reaction controls based on the conversion time expression for shrinking spheres using the stokes regime (small particles) [48].

In the shrinking sphere model, the reaction occurs within a spherical particle, and the rate at which the particle shrinks depends on whether the process is controlled by the diffusion of reactants to the particle surface (film diffusion control) or by the chemical reaction rate within the particle (reaction control). The expressions given describe the dimensionless time t/τ in relation to the conversion fraction X_B.

When the system is controlled by film diffusion and t/τ =0.999, been highest value, the conversion fraction X_B is approximately 0.999999. This indicates that the conversion is nearly complete. The small value of $1-X_B$ suggests that the shrinking sphere is almost entirely converted, and only a very small fraction remains unreacted [49]. Film diffusion is the limiting step, and the process is nearly at its maximum efficiency given the conditions. When the system is controlled by reaction rate and t/τ=0.973, the conversion fraction X_B is approximately 0.9999803. This indicates that the conversion is still very high but not as close to complete as in the film diffusion case [50]. The small difference from complete conversion reflects the fact that reaction control allows for a higher remaining fraction of the unreacted core compared to film diffusion control. The results from Table 4 suggest that under the given conditions, film diffusion control leads to nearly complete conversion, while reaction control achieves slightly lower, though still very high, conversion [51].

4. CONCLUSION

The study provides a detailed understanding of the mineral composition, optimal conditions for the dissolution of tantalite ore and shrinking core model of tantalite mineral under the following variable factors; acid concentration, temperature, stirring speed and particle diameters. These insights not only enhance our knowledge of the Okpella sample but also offer practical guidance for improving dissolution processes.

DISCLAIMER (ARTIFICIAL INTELLIGENCE)

Author(s) hereby declare that NO generative AI technologies such as Large Language Models (ChatGPT, COPILOT, etc.) and text-to-image generators have been used during the writing or editing of this manuscript.

ACKNOWLEDGEMENTS

The authors sincerely thank the members of the Analytical Research Laboratory, Faculty of Physical Sciences and the Chemistry Laboratory, Department of Science Laboratory Technology at the University of Benin, Benin City. Their gratitude also extends to Dr. Uwaifo Peter of the Benin-Owinna River Basin Development Authority Joint Analytical Research Laboratory for his support, cooperation, and access to laboratory facilities. Special thanks are due to Miss Favour Ehizode Okpiabele and Osahenrumwen Eva Samson, the research assistants, for their dedication and hard work during the bench work. Additionally, the authors are grateful for the insightful comments and suggestions from the anonymous reviewers and editor, which greatly improved the quality of the paper.

COMPETING INTERESTS

Authors have declared that no competing interests exist.

REFERENCES

1. Barsisa B, Amit KS. The Genesis of the Kenticha rare-metal granite-pegmatite, Sourthern Ethiopia. Mineralogy and Petrology. 2023;117(2):401-409.
2. Okuo JM. and Agho TI. A Preliminary survey of the lithochemistry of tantalite mineral from granitic pegmatite deposits in the Okpella area, Northern Edo state Nigeria. Journal of Material and Environmental Sustainability Research. 2024;4(2):39-46.
3. Palache C, Berman H, Frondel C. Dana's system of mineralogy, (7th edition). 1944,1;780–787.
4. Warr LN. IMA–CNMNC approved mineral symbols. Mineralogical Magazine. 2021;85(3):291–320
5. Miller GL. Tantalum and Niobium; *Butterworths Scientific Publications,* London. 12. Mineralogy and Petrology. 2000;1959:70: 165.
6. Arblaster JW. Selected values of the crystallographic properties of elements: Material park, Ohio: ASM International; 2018.
7. Melcher F, Sitnikova M, Graupner T, Oberthur T, Martin N. Fingerprinting of

conflict minerals: columbite-tantalite ("coltan") ore. Society for geology applied to mineral deposits. News Number. 2008;23.

8. Baba AA, Adekola FA, Faseki MA. Study of the kinetics of the dissolution of a Nigerian tantalite ore in hydrochloric acid. IFE Journal of Science. 2005;7(2):221 -236.
9. Baba AA, Dauda TO, Abdulkareem AY. Processing of a Nigerian columbite-rich ilmenite ore for improved industrial application by sulphuric acid solution. Indonesian Mining Journal. 2018; 21(1):9-19.
10. Olushola SA. and Folahan AA. Leaching of a Nigerian Columbite in Hydrochloric Acid: Dissolution Kinetics. International Journal of Metallurgical Engineering. 2012;1(3):35-39
11. Sanda O. and Taiwo EA. Investigation dissolution kinetics of a Nigeria columbite in Hdrofluoric acid using the shrinking core model. Nigerian journal of Technology. 2016;35(4):841-846
12. Alexander BW, Subhajyoti C, Thibault C, Christian U, Ekaterina L, Pragati P, Michael RG,Patrick JC, George CS. and Eric JS. Tantalum, easy as Pi: understanding differences in metal- imido bonding towards improving Ta/Nb separations. Chemical Sciences. 2022;13 (23):6796-6805.
13. Nishumura T, Sakrai H, Nagao S, Isu T, Alkasaka Y, Tsabouchi N. Recrystallization of silicon film on nitride/oxide double insulating structure by CW laser irradiation. Japanese Journal of Applied Physics. 1982;21(1):169-174.
14. Okuo JM, Agho TI. A Preliminary Survey of the Lithochemistry of Tantalite Mineral from Granitic Pegmatite Deposits in the Okpella Area, Northern Edo State, Nigeria. Journal of Materials and Environmental Sustainability Research. 2024;4(2):39 -46.
15. Stanislaus NN, Mokgalaka M, Maila N, Popoola P, Okanigbe D, Adeleke A, Adeosun S. Pyrometallurgical Approach in the Recovery of Niobium and Tantalum: Extraction Metallurgy- New Perspective, Intech Open. 2024;109025.
16. Neta M, Purcell W, Snyders E, Nel JT, Beukes G. Characterization and alternative dissolution of tantalite mineral samples from Mozambique. Journal of the Southern African Institute of Mining and Metellurgy. 2012;112(12):1079-1086.
17. Berhe GG, Alberto VDR, Tadesse B, Yimam A, Woldetinsae G. Decomposition of the Kenticha mangano-tantalite ore by HF/H_2SO_4 and KOH fusion. Physicochemical Problems of Mineral Processing. 2018;54(2):406-414.
18. Berhe GG, Cheru MS. Hydrometallurgical assessment of oxides of Nb, Ta, Th and U from Ethiopian tantalite ore. Heliyon. 2024;10(2):e24870.
19. Guo X, Wang D, Li Q. The Surface Structure Change of Columbite-(Fe) Dissolution in H_2SO_4. Minerals. 2023;13: 445.
20. Woldeselsassie EK, Aredo D, Mekonnen, T. Review on tantalum extraction by different method in Kenticha tantalum mine, Ethiopia. International Journal of Engineering & Technology Sciences. 2019;4:229-237.
21. Alhassan Y, Tsafe AI, Birnin-Yauri UA, Okunola OJ, Yargamji GI, Yebpella GG, Ndana M. EDXRF analysis of tantalite deposit of Mai-Kabanji, North-western Nigeria. Journal of Environmental Chemistry and Ecotoxicology. 2010;2(7): 117-119.
22. Alaoui A, El Kacemi K, El Ass K, Kitane S. Application of Box-Behnken design to determine the optimal conditions of reductive leaching of MnO_2 from manganese mine tailings. Russian Journal of Non-Ferrous. 2015;56:134-141
23. Abdulsalam J, Mulopo J, Bada S, Oboirien B, Falcon R. Experimental evaluation of activated carbon derived from South Africa discard coal for natural storage. International Journal of Coal Science and Technology. 2019;6:459-477.
24. Rutto H, Enweremadu C. Dissolution of a South African Calcium based Material using Urea: An Optimized Process. Korean Journal of Chemical Engineering. 2012;29 (1):1-16
25. Lizama HM, Fairweather MJ, Dai Z, AllegrettoTD. How does bioleaching start? Hydrometallurgy. 2003;69(1-3):109-116.
26. Baba AA, Adekola FA, Dele-Ige OI, Bale RB. Investigation of Dissolution Kinetics of a Nigerian Tantalite Ore in Nitric acid. Journal of Minerals and Materials

Characterization and Engineering. 2008;7 (1):83-95.

27. Okunlola OA. Regional metallogens of rare metals (Ta-Nb) mineralization of precambrain pegmatites of Nigeria in the Basement Complex of Nigeria and its mineral resources. A tribute to M.A.O. Rahaman, Akin Jinad and Co., Ibadan, Nigeria. 2006:107-128.
28. Teimouri, S. Feasibility Study on the Use of Imidazolium-Based Ionic Liquids in the Extraction of Gold. Master's Thesis, University of the Witwatersrand, Johannesburg, South Africa, 2020.
29. Whitcomb P. Exciting New Features in Design-Expert-V11 and Beyond. In Proceedings of the Stat-Ease European User Conference, Munich, Germany. 2018;4-6.
30. Bandara AMTS. and Senanayake, G. Leachability of rare-earth, calcium and minor metal ions from natural Fluorapatite in perchloric, hydrochloric, nitric and phosphoric acid solutions. Effect of proton activity and anion participation. Hydrometallurgy. 2015;153:179-189.
31. Wei X, Gao Y, Han J, Wang Y, Qin W. Optimization of extraction of valuable metals from waste LED via response surface method. Transaction of Nonferrous Metals Society of China. 2022; 33:938-950.
32. Soumya C, Naba KM, Biswajit D, Palas R, Bikash S. Biosorption of carbaryl from aqueous solution onto *Pistia stratiotes* biomass. Journal of Applied Water Science. 2013;4.
DOI: 10.1007/s13201-013-0132-z.
33. Mohamed OA, Masood SH, Bhowmik JL. Investigation of dynamic elastic deformation of parts processed by fused deposition modeling additive manufacturing. Advances in Production Engineering and Management Journal. 2016;13(3):227-238.
34. Belsley DA, Kuh E, Welsch RE. Regression diagnostics: Identifying influential data and sources of collinearity. John Wiley and Sons; 1980.
35. Li J. and Valliant R. Linear regression influence diagnostics for unclustered survey data. Journal of Official Statistics. 2011;27(1):99-119.
36. Yang X, Werner J, Honaker RQ. Leaching of rare Earth elements from an Illinois basin coal source. Journal of Rare Earths. 2019;37:312-321.
37. Li M, Zhang XW, Liu ZG, Wang MT, Liu J, Yang JP. Mixed rare earth concentrates leaching with HCl-$AlCl_3$ solution. Rare Metals. 2013;32:312-317.
38. Harrar H, Eterigho-Ikelegbe O, Modiga A, Bada S. Mineralogy and distribution of rare earth elements in the Waterberg coalfield high ash coals. Mineral Engineering. 2022, 183:107611.
39. Amine M, Asafar F, Bilali L, Nadifiyine M. Hydrochloric Acid Leaching Study of Rare Earth Elements from Moroccan Phosphate. Journal of Chemistry. 2019;1-6.
40. Ajemba RO. and Onukwuli OD. Application of the shrinking core model to the analysis of Alumina leaching from Ukpor Clay using nitric acid. International Journal of Engineering Research andTechnology. 2012;1(3):1-14.
41. Levenspiel O. Chemical Reaction Engineering, 2nd edition, Wiley, New York; 1972.
42. Gao G, Li D, Zhou Y, Sun X, Sun W. Kinetics of high-sulphur and high-arsenic refractory gold concentrate oxidation by dilute nitric acid under mild conditions. Mineral Engineering. 2009;22:111–115.
43. Faraji F, Alizadeh A, Rashchi F, Mostoufi, N. Kinetics of leaching: A review. Review Chemical Engineering. 2020;1:1–36.
44. Dickinson CF. and Heal GR. Solid-liquid diffusion controlled rate equations. Thermochim. Acta. 1999;340–341:89–103.
45. Papp JF. Minerals Year book Nb and Ta. US Geological Survey; 2006
46. Champion D. Australian Resources Reviews: Tantalum 2019. Geoscience Australia, Canberra; 2020.
47. United States Geological Survey. Mineral Commodity Summaries; 2019.
48. Global Tantalum market size and growth projections (CAGR); 2024- 2031
49. U.S. Geological Survey, Mineral Commodity Summaries, January 2024
50. Agho TI. and Archibong UD. Solvent Extraction of Bismuth (III) from Nitric Acid Solutions by Tri-n-butyl phosphate and Di (2-ethylhexyl) phosphoric acid. International Journal of ScientificResearch in Chemical Sciences. 2023;10(6):13-20.

51. Birniwa AH, Mohammad REA, Ali M, Rehman MF, Abdullahi SS, Eldin SM, Mamman S, Sadiq AC, Jagaba AH. Synthesis of Gum Arabic Magnetic Nanoparticles for Adsorptive Removal of Ciprofloxacin: Equilibrium, Kinetic, Thermodynamics Studies and Optimization by Response Surface Methodology. Separations. 2022;9: 322.

Disclaimer/Publisher's Note: The statements, opinions and data contained in all publications are solely those of the individual author(s) and contributor(s) and not of the publisher and/or the editor(s). This publisher and/or the editor(s) disclaim responsibility for any injury to people or property resulting from any ideas, methods, instructions or products referred to in the content.

© Copyright (2024): Author(s). The licensee is the journal publisher. This is an Open Access article distributed under the terms of the Creative Commons Attribution License (http://creativecommons.org/licenses/by/4.0), which permits unrestricted use, distribution, and reproduction in any medium, provided the original work is properly cited.

Peer-review history:
The peer review history for this paper can be accessed here:
https://www.sdiarticle5.com/review-history/123758